# CHEMICAL SYNTHESIS AND CHARACTERIZATION OF FUNCTIONALIZED MAGNETITE NANOPARTICLES FOR TARGETING BREAST CANCER CELLS AND TISSUES

A Thesis Submitted to the Department of Materials Science and Engineering

African University of Science and Technology

In Partial Fulfillment of the Requirements for the Degree of Master of Science.

By

Emmanuel Elias Gati

ID Number 40735

Abuja, Nigeria
April 2021

CHEMICAL SYNTHESIS AND CHARACTERIZATION OF FUNCTIONALIZED MAGNETITE NANOPARTICLES FOR TARGETING BREAST CANCER CELLS AND TISSUES

A THESIS APPROVED BY THE MATERIAL SCIENCE AND ENGINEERING

DEPARTMENT

RECOMMENDED: ----------

Supervisor, Prof Wole Soboyejo

---

Head, Department of Materials Science and Engineering

Professor A.P. Onwualu

APPROVED:

---

Chief Academic Officer

---

Date

April 2021



Emmanuel Elias Gati

## CERTIFICATION

This is to certify the thesis entitled **Chemical Synthesis and Characterization of Functionalized Magnetite Nanoparticles For the Targeting of Breast Cancer Cells and Tissues** submitted for a Master's degree at the African University of Science and Technology (AUST) School of Postgraduate Studies, Abuja, Nigeria, is a record of the original research performed in Abuja, Nigeria, carried out by **Emmanuel Elias Gati** in the department of Materials Science and Engineering.

## ABSTRACT

This study presents the results of the characterization of functionalized magnetite nanoparticles for targeting breast cancer cells. In this study, spherical magnetite nanoparticles with core diameters between 5nm and 30 nm were chemically synthesized by the co-precipitation method from ferric and ferrous salts under inert conditions and ambient temperature. The sizes and shapes of the magnetite nanoparticles (MNPs) were determined by the Transmission Electron Microscopy (TEM). The sizes of the MNPs were within the range recommended for biomedical applications such as contrast enhancement in magnetic resonance imaging (MRI). The synthesized MNPs were conjugated to LHRH and EphA2, which are known targets of receptors that are overexpressed on the surfaces of breast tumors. They were then analyzed using Energy-dispersive X-ray spectroscopy (EDS), which indicated two large peaks for iron and oxygen as the main two-element composition in the synthesized nanoparticles. A Vibrating Sample Magnetometer (VSM) was then used to characterize the magnetic properties of synthesized nanoparticles. This revealed a very small saturation magnetization of 2.67 emu/g, compared to that of bulk iron oxide 92emu/g. FTIR spectra of the LHRH- and EphA2-conjugated nanoparticles revealed strong broader peaks of 3356 $cm^{-1}$ for the amine ($–NH_2$) and characteristic peaks for both LHRH and EphA2. The amide (-C=O) peak at 1646 $cm^{-1}$ revealed that EphA2 was properly conjugated to magnetite nanoparticles (MNPs). Analysis of the synthesized nanoparticles using UV-vis spectroscopy showed the broad peak for pure MNPs, and the peaks of both LHRH and EphA2 conjugated nanoparticles. These were found to be between 262nm and 400nm, which is within the visible range of wavelengths for nanoparticles that are being developed for cancer detection and treatment.



**Key words:** Magnetite nanoparticles (MNPs), iron (III) oxide, Energy dispersive spectroscopy (EDS), Fourier Transform Infrared Spectroscopy (FT-IR), Transmission Electron Microscopy (TEM), UV/VIS spectroscopy, Vibrating Sample Magnetometer (VSM).

## DEDICATION

This Master of Science thesis is dedicated to my late father, Elias Gati, who supported me financially from elementary school to undergraduate level, and encouraged me in my early schooling. May his soul rest in eternal peace.

## TABLE OF CONTENTS

## LIST OF FIGURES

## LIST OF EQUATIONS

## ACKNOWLEDGEMENT

Thanks to God for the privilege and gift of life to have completed this Master's degree program in Material Science and Engineering. I thank, my supervisor, Prof Wole Soboyejo for his support, encouragement, and counsel. Much appreciation to Madam Theresa Ezenwafor, a Ph.D. student and Biomaterials Teaching Assistant, for her assistance with laboratory work at WPI, in USA. Thanks also to Mr. Chukwudi Ezeala (Ph.D. student) at AUST for incredible support while doing laboratory work. Without them, my work could have not reached this end. Thanks to the M.Sc. program scholarship sponsors, Pan African Materials Institute (PAMI), for their financial support throughout the study. Appreciation to all AUST faculty members and my colleagues in the Department of Material Science and Engineering. Besides, I extend my appreciation to my beloved wife, Madam Lightness Macha, and my daughters, since I spent time preparing the project rather than taking care of them as a responsible father. Thanks to my mother, Sophia Elias, for her love, support and encouragement during my work on this project.

# CHAPTER ONE

# INTRODUCTION

## 1.1 Introduction

Cancer is a term used to describe a group of diseases in which abnormal cells develop and spread uncontrollably (Section & Epidemic, 2018). It is possible to die if the spread is not managed. Cancer kills one out of every six people on the planet, more than AIDS, tuberculosis, and malaria combined. It is now the second leading cause of death worldwide (after cardiovascular diseases) and in countries with a high or very high Human Development Index (HDI) (Section & Epidemic, 2018). According to the International Agency for Research on Cancer (IARC), 17.0 million new cancer cases were diagnosed worldwide in 2018.

However, due to the rising prevalence of risk factors such as smoking, poor diet, physical inactivity, occupational exposures, environmental factors, and fewer pregnancies, the potential cancer burden would almost certainly be much higher. Lung, breast, and colorectal cancers, which are linked to these causes, are already on the rise in economically transitioning countries, and this trend will continue if preventive measures are not widely implemented (Section & Epidemic, 2018).

“Breast cancer is a pathology that emerges from the breast tissue, especially the milk duct (ductal carcinoma representing 80% of the cases) as well as the lobules. Cancer emerging from the ductile region is known as ductal carcinoma while those emerging from the mammary lobules are known as lobular carcinomas (Medina et al., 2020)”

Breast cancer is the most frequently diagnosed cancer in women worldwide with more than 2 million new cases diagnosed in 2018, accounting for 25% of all new cancer cases in women. (Section & Epidemic, 2018). Breast cancer is a prevalent condition in both developing and developed countries, and it is the second leading cause of death in Europe and the United States, after lung cancer (Medina et al., 2020).

Triple-Negative Breast Cancer (TNBC) is so-called because it lacks estrogen receptors, progesterone receptors, and overexpression of the growth-promoting protein HER2. It makes up only 15 to 20 percent of all breast cancers and is characterized by shorter overall survival and an early peak of distant recurrences at 3 years after diagnosis. (Shekar et al., 2020). TNBCs are difficult to diagnose and treat with traditional hormone therapy, such as aromatase inhibitors and tamoxifen, and some chemotherapy medications, such as Herceptin (trastuzumab), because some breast cancer diagnosis and treatment schemes target estrogen, progesterone, and HER2 receptors (Slamon et al., 2001); (Gelmon et al., 2015); (Andersson et al., 2011). There is, therefore a need for novel approaches to the early detection and treatment of triple-negative breast cancer. The majority of deaths occur in the first 5 years following initial diagnosis. Late tumor recurrences are unusual with this breast cancer subtype and recurrences generally are not observed after 8 years (Collignon et al., 2016).

Nanotechnology is a widely used area for specific detection of cancer cells and target delivery of drugs for cancer treatment (Ganapathe et al., 2020). Nanoparticles from silver, gold, and magnetite have shown potential results in the diagnosis and treatment of diseases.

Magnetite nanoparticles are small synthetic or $Fe_3O_4$ (magnetite) particles with a core varying between 10 nm and 100 nm in diameter. These magnetite nanoparticles are coated with certain biocompatible polymers, such as dextran or polyethylene glycol, which provide chemical handles for the conjugation of therapeutic agents and also enhance their blood distribution profile (Hoffmann et al., 2005).

Magnetic nanoparticles (MNPs) have attracted considerable attention for various biomedical applications (Press, 2012);(Hoffmann et al., 2005); (Wahajuddin& Arora, 2012);(Stephen et al., 2011) including nanocarriers for biochemical molecules or drug delivery, heat mediators in hyperthermia, and contrast-imaging agents in magnetic resonance imaging (MRI) and magnetic targeting. In these applications, MNPs of homogenous size and uniform shape is desired (Ganapathe et al., 2020). Superparamagnetic MNPs exhibit a zero average magnetization in the absence of an external magnetic field against agglomeration of MNPs caused by intermolecular interaction (Wahajuddin & Arora, 2012).

Luteinizing hormone-releasing hormones (LHRH) and EphA2 receptor antibody which are over-expressed in cancer tumors are potential carriers of the nanoparticles and drug delivery agents. There are significant studies on the potential of Luteinizing hormone-releasing hormone (LHRH) conjugated to magnetic nanoparticles (MNPs-LHRH) and EphA2 conjugated to magnetic nanoparticles (MNPs-EphA2) as a contrast agent in MRI imaging of cancer cells.

A study conducted by Obayemi et al (2016) shows that biosynthesized magnetic nanoparticles have high adhesion force to both breast cancer cells and normal breast cells than chemically synthesized magnetic nanoparticles. Furthermore, the study showed that adhesion of LHRH-conjugated BMNPs or BSA-conjugated BMNPs to cancer cells is shown to be 6 times greater than that of normal breast cells. This value suggests that LHRH-conjugated BMNPs have the potential for the specific targeting of breast cancer cells/tissue. (John D. Obayemi et al., 2017).

The increase in adhesion forces between luteinizing hormone-releasing hormone, LHRH- or EphA2, a breast specific antibody(BSA)-conjugated BMNPs to breast cancer cells is attributed to van der Waals interactions between the peptides/antibodies from the conjugated nanoparticles and the over-expressed receptors (revealed using immunofluorescence staining) on the surfaces of the breast cancer (John D. Obayemi et al., 2017).

Other studies have shown the applicability of LHRH-MNPs contrast agents for the specific detection of cancer through targeted magnetic resonance imaging (MRI) (Jingjie Hu et al., 2020). Zhou et al., 2006 conducted a study on In vivo distribution of magnetic nanoparticles conjugated with Luteinizing Hormone-Releasing Hormone in mice bearing breast cancer tumors were studied using TEM analysis. Results suggest that LHRH conjugated magnetic nanoparticles target both primary breast cancer cells and their resulting metastases in other organs (lung in this study). Furthermore, the accumulation of individual nanoparticles in the nucleus of liver cells suggests that LHRH-MNPs are potential carriers for delivering drugs or DNA to liver cells with diseases.

The study on synthesis and characterization of monodispersed water-dispersible $Fe_3O_4$ nanoparticles and in vitro studies on human breast carcinoma cell lines under hyperthermia conditions suggests that the water-dispersible $Fe_3O_4$ MNPs will be a potential candidate material for application in magnetic-based hyperthermia therapy (Sharma et al., 2018). Thus, this study explores the chemical synthesis and characterization of functionalized magnetite nanoparticles for the targeting of breast cancer cells and tissues. The results from this study will form a basis for comparison of the characterization of nanoparticles and conjugated nanoparticles using both distilled water (pH=5.8) and phosphate-buffered saline, PBS (pH=7.2) solvents.

## 1.2 Objectives

### 1.2.1 General Objectives

The general objective of this study was chemical synthesis and characterization of functionalized LHRH and EphA2 conjugated MNPS for specific targeting of breast cancer cells and tissues.

### 1.2.2 Specific Objectives

The specific objectives of this study include:

i. The chemical synthesis of magnetic nanoparticles (MNPs) by co-precipitation method
ii. The PEGylation (functionalization) of chemically synthesized Magnetic nanoparticles
iii. LHRH and EphA2 Conjugation to MNPS for specific detection of breast cancer cells.

## 1.3 Scope of Work

The study will focus on the chemical synthesis and characterization of functionalized magnetic nanoparticles for specific targeting of breast cancer cells and tissues. In this study, magnetic nanoparticles were chemically synthesized by the co-precipitation method and functionalized by coating to polyethylene glycol (PEG). The synthesized nanoparticles are conjugated to LHRH and EphA2 over expressed receptors.

Other researchers have studied the interaction force between the LHRH conjugated to Biosynthesized magnetic nanoparticles (BMNPS). However, there have been no prior study of the effects of water and Phosphate Buffered Saline (PBS) on the chemical synthesis and structure of functionalized magnetite nanoparticles. These will be explored in this study using particles that were produced by the co-precipitation method.

## 1.4 Justification for the Study

"Unlike other cancers which are hormone receptor or HER2 positive, TNBC has no targeted treatments, so patients must rely only on surgery, chemotherapy, and radiation, which are less effective than targeted treatments and can harm healthy tissue (Collignon et al., 2016)". Cancer deaths are expected to outnumber those caused by AIDS, tuberculosis, and malaria combined each year. The most difficult aspect of cancer is early detection before it spreads, as well as the side effects associated with current treatment options.

A mammary tumor is the second leading cause of cancer death in women (Nazário et al., 2015). Breast cancer has the potentials to spread out in the body and form metastases in almost any vital organs and lymphatic system. The micrometastases may develop even after the removal of the primary tumor (Anders & Carey, 2009).

It is, therefore, important to detect breast cancers in the early stage. It has been shown that biocompatible magnetic nanoparticles (MNPs) can be used to improve cancer diagnostics and treatment (Wahajuddin& Arora, 2012);(Hoffmann et al., 2005). These include magnetic drug targeting (Wahajuddin & Arora, 2012), hyperthermia (Wahajuddin & Arora, 2012), magnetic field-assisted radionuclide therapy, and magnetic resonance imaging (MRI) contrast enhancement (Stephen et al., 2011).

The spatial resolution of the approaches commonly used to diagnose cancer limits the early detection approach for breast cancer. Existing breast cancer screening techniques (mammograms, ultrasound, magnetic resonance imaging (MRI), and various forms of scans) are unsuccessful at detecting cancer in its early stages. Hence, the diagnosis is often too late for the current treatments to be efficacious (Gegechkori et al., 2017). Most patients that undergo the common bulk systemic cancer treatment, often experience excruciating pain, with significant short and long-term side effects (Gegechkori et al., 2017). These treatments are also associated with high costs.

This, therefore, has stimulated the need for novel approaches for the detection and treatment of cancer cells before and after metastases. This stimulated our recent efforts in the development of functionalized magnetite nanoparticles for the early detection and treatment of cancer (Hampp et al., 2012). The biocompatible nanoparticles developed are functionalized with some molecular recognizing units (MRUs) (Meng et al., 2009); (Zhou et al., 2006).

When these functionalized nanoparticles are injected into the bloodstream, they can diffuse through the capillaries and pores, until they reach receptors on cancer cells that can bind specifically to MRUs (such as antibodies and peptides) that are attached to nanoparticles (Wahajuddin & Arora, 2012).

Many studies have been done on LHRH-MNPS as a negative contrast agent using Magnetic Resonance Imaging (MRI) for specific detection of cancer cells. However, no significant work has been done on the Chemical synthesis and characterization of MNPs conjugated to both LHRH and/or EphA2 for specific detection of breast cancer. This study will therefore determine the potential of chemical synthesis and characterization of both LHRH/EphA2 conjugated MNPs for targeting breast cancer cells.

# CHAPTER TWO

# LITERATURE REVIEW

## 2.1 Introduction

In this section cancer and breast cancer-related issues will be discussed. Methods on the detection and treatment of cancer will be included also. The review of underlying experimental methods will be presented in the last subsection.

## 2.2 Global Review of Cancer

Every year, an estimated 1 million new cases of breast cancer are discovered around the world. Around 170,000 of these have triple-negative breast cancer (Ismail-khan & Bui, 2014). Basal-like breast cancer refers to the molecular phenotype of the tumor as described by cDNA microarrays, which accounts for around 75% of TNBC cases.

TNBC is most common in premenopausal African American women; according to a recent study, TNBC affects 39% of all African American premenopausal women diagnosed with breast cancer (Ismail-khan & Bui, 2014).

## 2.3 Background on Cancer

Cancer survival is affected by factors such as the type of cancer that occurs, the stage at which they are diagnosed, the prevalence of screening/early detection services, and whether treatment is available. “Several different staging systems are used to classify cancer. If cancer cells are present only in the layers of cells where they developed the stage is in situ. If cancer cells have penetrated beyond the original layer of tissue, cancer has become invasive and is categorized as local, regional, or distant based on the extent of spread. (*Advanced Breast Cancer : Diagnosis and Treatment*, 2020)”

Breast cancer is the leading cause of cancer death among women around the world, with an estimated 626,700 women dying from the disease in 2018. By detecting and removing precancerous lesions, screening can help prevent colorectal and cervical cancers. Breast, colorectum, cervix, and lung cancers can all be detected early when treatment is more likely to be effective, and screening can help minimize mortality (among long-term current or former heavy smokers) (Section & Epidemic, 2018).

A lump or mass in the breast is one of the most common signs and symptoms of breast cancer. Other signs include persistent changes to the breast, such as thickening, swelling, distortion, tenderness, skin irritation, redness, scaliness, and nipple abnormalities or spontaneous nipple discharge, as well as skin irritation, redness, scaliness, and nipple abnormalities or spontaneous nipple discharge. Breast cancer in its early stages normally has no symptoms and is diagnosed by mammography screening (Section & Epidemic, 2018).

The first step to cancer management and diagnosis includes a careful clinical and pathological assessment. Once a diagnosis is confirmed, cancer must be staged to determine treatment options and prognosis, and to apply the appropriate treatment protocols.(*Advanced Breast Cancer : Diagnosis and Treatment*, 2020).The primary modalities of cancer treatment are surgery, chemotherapy, radiotherapy, hormone therapy, immune therapy, and targeted therapy. The majority of cancer patients are diagnosed with advanced-stage disease (Nazário et al., 2015).

## 2.4 Methods for Detection and Treatment of Cancer

TNBCs are biologically aggressive; although some reports suggest that they respond to chemotherapy better than other types of breast cancer, prognosis remains poor. This is due to two factors: shortened disease-free intervals in the adjuvant and neoadjuvant setting and a more aggressive clinical course in the metastatic setting (Ismail-khan & Bui, 2014).

The most popular clinical imaging and detection modalities used for breast cancer detection are X-ray mammography, magnetic resonance imaging (MRI), and ultrasound scanning. Breast cancer is also diagnosed by microwave imaging (Aldhaeebi et al., 2020).

Traditional breast cancer screening methods, such as X-ray mammography, magnetic resonance imaging, and ultrasound scanning, have drawbacks such as high costs, harmful radiation, and inconveniences to the patients (Aldhaeebi et al., 2020). The conventional treatments include surgery, radiation, chemotherapy, hormone therapy, immune therapy, and targeted therapy (drugs that specifically interfere with cancer cell growth) (Shekar et al., 2020). The conventional treatment of cancer can affect the body systems, such as blood circulation, lymphatic and immune systems, and the hormone system (Anders & Carey, 2009).

Mammography is the only USFDA approved exam to be used for screening breast cancer in women with no prior symptoms. Mammography, however, has recently been subjected to immense scrutiny because of comparatively high false negative and false positive tests that can prove to be. Furthermore, because of the ionizing radiation associated with X-rays, people who use mammography as a screening tool have a higher risk of developing cancer (Medina et al., 2020).

Another method of breast cancer detection is Ultrasound screening where sound waves are transmitted through a transducer, which sends pulses into the breast and detects echoes from inside the breast; these echoes are used to form ultrasound images. Ultrasound, on the other hand, is not suitable for breast imaging due to its low resolution and inability to differentiate between malignant and benign breast tumors (Medina et al., 2020). The microwave imaging (MI) method can detect small breast tumors since it is based on the electrical properties' contrast between normal and tumor breast tissues (Aldhaeebi et al., 2020). These problems include unreliable in vivo contrast estimation, measurement system uncertainties, and results that do not comply with other standard detection methods.

With the development of the nanotechnology field and nanomaterials, several studies (Hernández-Hernández et al., 2020) suggested and explored the possibility of improving the available cancer detection methods (magnetic resonance imaging (MRI), magneto-acoustic tomography (MAT), computed tomography (CT), and near-infrared (NIR) imaging)by integrating a biocompatible detection system with magnetic nanoparticle materials (Aldhaeebi et al., 2020). Magnetic nanoparticles (MNPs) have drawn a lot of interest for a variety of biomedical applications (Stephen et al., 2011), such as nanocarriers for biochemical molecules or drug delivery, heat mediators in hyperthermia, and contrast-imaging agents in MRI and magnetic targeting. MNPs of uniform size and shape are favoured in these applications (Hoffmann et al., 2005).

According to the Studies conducted by (Jingjie Hu et al., 2020); John Obayemi (2020) the ability of LHRH-MNPs as a negative contrast agent for the specific detection of TNBC has been demonstrated. In an experimental study, LHRH-MNPs appeared to darken breast

tumors 24 hours after injection for intravenous administration, although contrast enhancement was not apparent in animals injected with only MNPs. According to these results, the targeted LHRH-MNPs concentrated in various vital organs in non-tumor-bearing mice, including the liver, spleen, and kidney.

Another study conducted by (John D. Obayemi et al., 2017) shows that biosynthesized magnetic nanoparticles (BMNPS) has high adhesion force to both breast cancer cells and normal breast cells than chemically synthesized magnetic nanoparticles. Furthermore, the adhesion of LHRH-conjugated BMNPs or BSA-conjugated BMNPs to cancer cells is 6 times greater than that of normal breast cells, according to the report. This significance indicates that LHRH-conjugated BMNPs could be used to target breast cancer cells and tissue specifically. Other studies have shown the applicability of LHRH-MNPs contrast agents for the specific detection of cancer through targeted magnetic resonance imaging (MRI) (Jingjie Hu et al., 2020). The results of the study showed that there was a significant increase of LHRH-MNPs uptake and retention in cancer cells than when compared with MNPs targeting only.

### 2.5 Magnetite Nanoparticles Review

The magnetite nanoparticles are used as contrast agents in MRI due to the combined advantages of their magnetic properties, biocompatibility, and applicability to in vivo studies (Revia & Zhang, 2016); (Bao et al., 2018); (Stephen et al., 2011).

As magnetite nanoparticles are injected into the body, they produce an additional magnetic field (due to an external magnetic field, such as MRI) that attracts hydrogen protons in the

vicinity (Stephen and colleagues, 2011). Protons in the vicinity have a shorter relaxation time as a result of the combined magnetic moments (Revia& Zhang, 2016).

Several methods are used for the synthesis of magnetite nanoparticles which include; co-precipitation, thermal decomposition, hydrothermal and solvothermal synthesis. Other methods are microemulsion, ultrasound-assisted methods, microwave-assisted methods, and green synthesis (Hernández-Hernández et al., 2020). Due to the high yield of nanoparticles and the ease with which the co-precipitation process can be scaled up, it is one of the most commonly used methods in the synthesis of MNPs (Hernández-Hernández et al., 2020).

Several experiments have examined the adhesion of LHRH-MNPs to breast cancer cells and normal breast cells. According to Hu et al., 2020, the adhesion measured between LHRH-MNPs and TNBC cells was significantly greater than the adhesion measured between unmodified MNPs and TNBC cells.

The ability of LHRH-MNPs to bind to human TNBC cells has been discovered to be exceptional. Because of the enhanced adhesive interaction triggered by receptor-ligand specificity, LHRH-MNPs enter TNBC cells through receptor-mediated endocytosis. Unlike MNPs, LHRH conjugated MNPs are used as contrast agents in cancer cell detection and recognition.

Other results on LHRH-MNPs as MRI contrast agent for breast cancer imaging found that LHRH-MNPs injected intratumorally retained T2 signals in breast tumors for two weeks, demonstrating long-term tumor enhancement potential, while MNPs signal began to

recover to the contrast of the original tumor before injection at 24 hours post-injection. LHRH-MNPs darkened breast tumors 24 hours after intravenous administration, while contrast enhancement was not apparent in MNP-injected specimens. These findings demonstrate the utility of LHRH-MNPs as negative contrast agents for the specific detection of TNBC (Jingjie Hu et al., 2020).

Magnetite nanoparticles mainly reduce the T2 relaxation times of the tissues in which they accumulate and result in negative contrast (darkening) on T2 weighted images that are commonly used for the enhanced visualization and the identification of diseased tissues (Stephen et al., 2011).

**2.6 Review of Experimental Methods**

Obayemi et al successfully biosynthesized magnetite nanoparticles, which has resulted in the formation of the particle with clinical sizes between 10 nm and 60 nm. These biocompatible magnetic nanoparticles are produced in the presence of *Magnetospirillum magneticum* (MM) bacteria that respond to magnetic fields. The dependence of the synthesized nanoparticle structure, shape, and size on pH and time were characterized using a combination of transmission electron microscopy (TEM), environmental scanning electron microscopy (ESEM), UV-visible spectrophotometry (UV-Vis), and x-ray diffraction (XRD) (J D Obayemi et al., 2015).

Carbodiimide reduction with luteinizing hormone-releasing hormone (LHRH), a ligand whose receptors are overexpressed in most breast cancer cells (Zhang et al., 2004), also functionalized the particles generated. Fourier transform infrared (FTIR) and quantitative image processing were used to analyze the resulting particles.

The findings indicate that these particles may be used for specific targeting and to enrich magnetic resonance imaging (MRI) images in cancer and arteriosclerosis early detection and localized treatment (Anuku et al., 2020).

Enhanced cellular intake of LHRH-conjugated PEG-coated magnetite nanoparticles for selective targeting of triple-negative breast cancer cells was investigated in this study (Jingjie Hu et al., 2018). The PEG-coated MNPs had circular forms, with an average core diameter of about 30 nm, as shown by TEM images. The surface chemistry of the nanoparticles was investigated using Fourier Transform Infrared Spectroscopy (FTIR). MNPs, glutaraldehyde-activated MNPs, and LHRH-conjugated MNPs all had peaks that were similar to PEG-coated iron oxide in their FTIR spectra (Gupta & Wells, 2004); (Zhang & Zhang, 2005); (Zhang et al., 2002).

Among them were the Fe-O bond at 590 $cm^{-1}$ and the O-H group on the particle surface at 3300 $cm^{-1}$. Peaks at 1010, 1076, 1107, and 1153 $cm^{-1}$ reflect the C-O-C and C-H bonds in PEG. The $Fe_3O_4$ core of the magnetite nanoparticles used in this analysis is coated with PEG. The MNPs' surfaces have functional amine groups that enable LHRH peptides to be conjugated to these PEG-coated MNPs (J Hu et al., 2018); (Jingjie Hu et al., 2020).

A TEM analysis of functionalized magnetic nanoparticles targeting breast cancer cells revealed that TEM can be used to investigate the subcellular distribution of functionalized magnetic nanoparticles in mice with breast cancer (Zhou et al., 2006). The researchers discovered that dispersed LHRH-MNPs were found in tumor cells, as well as cells in the lungs and livers.

In kidney cells, no LHRH-MNPs were identified. Furthermore, LHRH-MNPs tend to aggregate and form clusters in tumor cells and cells in the lungs where metastases were developed. These suggest that MNPs functionalized using LHRH can be used to target both primary cancer cells and metastatic cells.

In 2018, Hu et al investigated the adhesion of LHRH agonist-conjugated PEG-coated magnetite nanoparticles to breast cells using a combination of experimental and analytical methods. A mixture of atomic force microscopy and molecular dynamics simulations are used to assess the adhesive association of ligand-conjugated nanoparticles with cells in vitro (Jingjie Hu et al., 2018). LHRH-magnetic nanoparticles (MNPs) have a greater adhesion to breast cancer cells than normal breast cells, according to their findings (Anuku et al., 2020). Therefore, the presence of triptorelin/LHRH molecules leads to increased specificity during the targeting of breast cancer cells. This increase in specificity was attributed to the increased incidence of over-expressed LHRH receptors on the surfaces of breast cancer cells. This study concludes that the work of adhesion between triptorelin-MNP-coated AFM tips and breast cancer cells is 14 times more than the work of adhesion between triptorelin-MNP-coated AFM tips and normal breast cells (Anuku et al., 2020).

Obayemi et al. (2017) discovered that the average adhesion forces between ligand-conjugated BMNPs-LHRH coated-AFM tips and MDA-MB-231 triple-negative breast cancer (TNBC) cells are over six times greater than normal breast cells in their sample. The enhanced adhesion of LHRH-conjugated or EphA2- conjugated MNPs to TNBC cells was due to the increased occurrence of LHRH and EphA2 receptors on the surfaces of breast cancer cells, according to the researchers (Anuku et al., 2020).

# CHAPTER THREE

# RESEARCH MATERIALS AND METHODS

## 3.1 Introduction

This chapter presents the materials and chemicals used, materials characterization methods, and experimental protocols that were used during the synthesis and conjugation of magnetite nanoparticles.

## 3.2 Materials

### 3.2.1 Equipment and Glassware

Some of the important laboratory apparatus used includes; nitrogen gas cylinder, three necks round-bottomed flask, micropipette, beaker, syringe, test tubes, test tube rack, test tube holder, hot plate, vacuum oven, shaker, centrifuge machine, magnetic stirrer, magnetic bar, spatula.

### 3.2.2 Chemicals and Reagents

All solvents were dried before use. Ferric chloride (99%), oleic acid (90%), Ferrous chloride (99%), Sodium hydroxide (NaOH), distilled water, Luteinizing hormone-releasing- hormone (LHRH), and Ephrine receptor $A_2$ (EpHA2). Other reagents include MT-PEG, CT-PEG, N-hydroxysuccinimide (NHS), EDS, phosphate-buffered saline (PBS). NHS and EDS were purchased from Thermofisher, Waltham, MA, USA, while EphA2 and LHRH from Invitrogen and BACHEM, Torrence, CA, respectively.

### 3.3 Materials Characterization

#### 3.3.1 Ultraviolet-Visible Spectroscopy

Ultraviolet-visible light spectroscopy more commonly referred to as UV-Vis spectroscopy is a technique used in analytical chemistry applications to characterize materials.

Light sources are used either one or two, to emit light over the ultraviolet and visible light spectra (200-800nm) (Helms, 1983). The concentration of the analyte within the sample is calculated by the equation Beer-Lambert law. This gives:

$$Absorbance = -log_{10}\left(\frac{l}{lo}\right) = concentration.\varepsilon.l$$ Equation 1: Beer Lambert Law

Where $\mathbf{I_0}$ is the incident light, **I** is the transmitted light, **ε** is the molar extinction coefficient of the analyte and **L** is the path length which is the distance traveled by light through the cuvette(Helms, 1983). The UV-vis spectroscopy was used to study the optical property of both synthesized nanoparticles and LHRH/ EphA2 conjugated nanoparticles.

In this study, 3mg of nanoparticles were measured and 5mls of distilled water was added. The mixture solution was sonicated and characterized by UV-Vis spectroscopy using water (pH=5.8) and phosphate-buffered saline (pH=7.2 separately. The data were collected using Specord: 200Plus (Analytic Jena, Made in Germany). UV-vis spectroscope graph was plotted by using origin lab software package version 2019 (9.65)

#### 3.3.2 Fourier Transform Infrared Spectrometry

Fourier Transform Infrared (FTIR) is a characterization technique with the ability to identify materials and determine the quality of a sample. This method identifies materials by the “fingerprints” of molecules as each FTIR spectrum is unique to the measured molecules. The Fourier transform is performed manipulating the data so that it can easily

be read and compared to other spectra for the determination of the compound functional group (Helms, 1983).

The conjugation process was elucidated using Fourier Transform Infrared (FTIR) Spectroscopy. Spectra were acquired using Nicolet iS5 ID1 Transmission (Thermo Scientific, USA). FTIR spectra were plotted using Origin Lab software package version 2019 b (9.65).

### 3.3.3 Transmission Electron Microscopy (TEM)

The size and morphology of $Fe_3O_4$ particles are investigated by Transmission Electron Microscopy (TEM). Transmission electron microscopy a technique that utilizes electrons as a light source to create extremely high-resolution images of samples. TEM uses a tungsten filament to send electrons through a vacuum column within the microscope to the sample (Helms, 1983).

In this study 50 µl nanoparticles suspensions (MNPs, LHRH-MNPs, EphA2-MNPs) were separately placed onto Transmission Electron Microscopy (TEM) grids (Electron Microscopy Sciences, CF300-Cu, Hatfield, PA, USA) that were studied in Philips CM100 TEM (Philips, Amsterdam, Netherlands). The core diameter of nanoparticles was determined by analyzing TEM micrographs with the Image J software package.

### 3.3.4 Vibrating Sample Magnetometry

The magnetic property of the synthesized nanoparticles was determined using a vibrating sample magnetometer (VSM), (Model 740 VSM, Lake Shore Cryotronics, Inc., Westerville, Ohio, USA). During VSM analysis, 0.5 mg of the samples were placed on a silicon wafer with a cross-sectional area of 5× 5 mm (J D Obayemi et al., 2015).

**3.3.5 Energy Dispersive X-ray Spectroscopy (EDS):** This was used to analyze the elemental composition of synthesized nanoparticles (Model Evo LS 10, Carl Zeiss, Berlin, Germany).

### 3.4 Experimental Procedures

#### 3.4.1 Magnetite Nanoparticle Synthesis

Synthesis of pure $Fe_30_2$ nanoparticles was done by co-precipitation method of ferric and ferrous salts were reacted in the oxygen-free atmosphere at ambient temperature. 3mg of $Fe_20_3$ and 3mg $Fe_30_2$ were measured separately using analytical balance followed by the addition of 50 mls of distilled water in a beaker that contains $Fe_20_3$ and $Fe_30_2$.

**Figure 1: Synthesis of magnetite nanoparticles**

The mixture was made homogenous using a magnetic stirrer for 30 minutes. The mixture solution was transferred into a three-necked round-bottomed flask and covered using a lid and left one hole to be connected to the $N_2$ cylinder.0.1 ml oleic acid was added to prevent further oxidation of magnetite to hematite. While the three-neck round-bottomed flask on

the hot plate sodium hydroxide (NaOH) was added drop by drop using a pipette to form black precipitate (magnetite). The addition of Sodium hydroxide was stopped and stirred for at least 5 minutes under Nitrogen gas conditions. The contents were allowed to cool for at least 20 minutes under room temperature.

The resulting magnetite nanoparticles were washed using distilled water and ethanol several times until all the sodium salts were completely removed by testing the pH to 7. The nanoparticles formed were dried using a vacuum oven at $60^0$C for 1 day to obtain black nanoparticles.


**Figure 2: Magnetic separation of synthesized nanoparticles**

$2FeCl_{3(s)} + FeCl_{2(s)} + 8NH_3 + 4H_20 \rightarrow Fe_3O_{4(S)} + 8NH_4Cl$

Equation 2: Chemical equation for iron oxide synthesis

Ionically

$Fe^{3+} + Fe^{2+} \rightarrow Fe_30_{4(S)}$

Equation 3: Ionic equation for the iron oxide synthesis

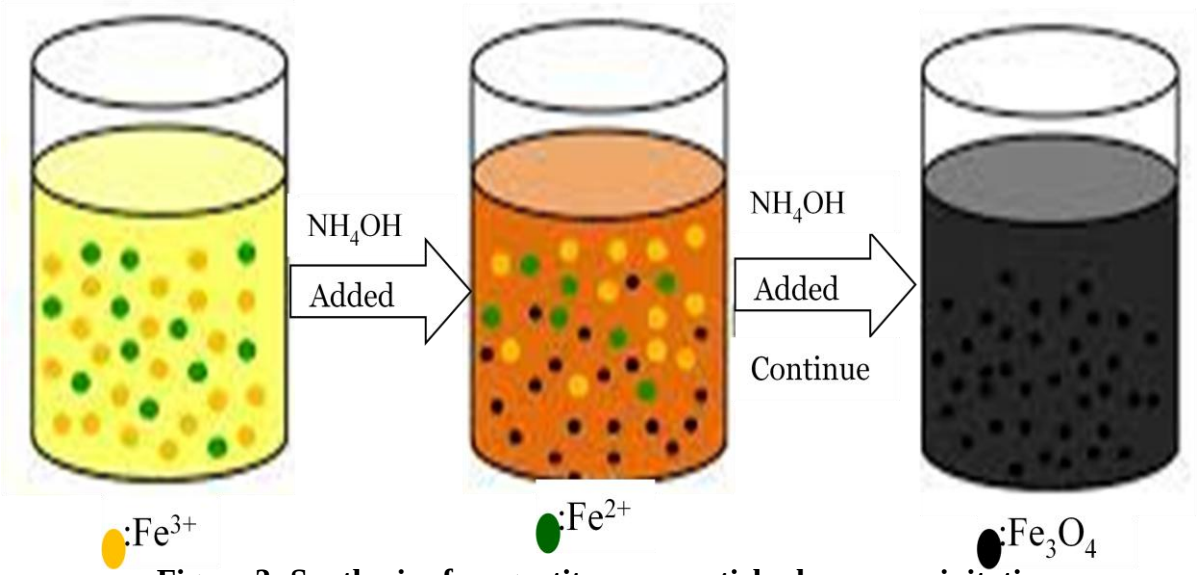


**Figure 3: Synthesis of magnetite nanoparticles by co-precipitation**

### 3.5 Pegylation of MNPs Procedures

Magnetic nanoparticles were coated with PEG-based on the following protocol. A known weight of magnetite nanoparticles was measured using balance followed by the addition of Phosphate-buffered solution (PBS). The mixture was sonicated for 30 minutes to allow homogenous mixing of the solution. The mixture solution was decanted to remove any particles that may settle at the bottom.

The solution was divided into two portions in different test tubes each 2.5mls (solution A and B). PBS was added to the mixture solution to make each one up to 5mls. An equal volume of CT-PEG and MT-PEG was added to solution A. The contents were transferred and placed on the shaker and allowed to react for 2 hours. The solution was centrifuged at

the speed of 1500rpm for 5 minutes. The above contents were analyzed using UV-vis spectroscopy and FTIR spectroscopy.

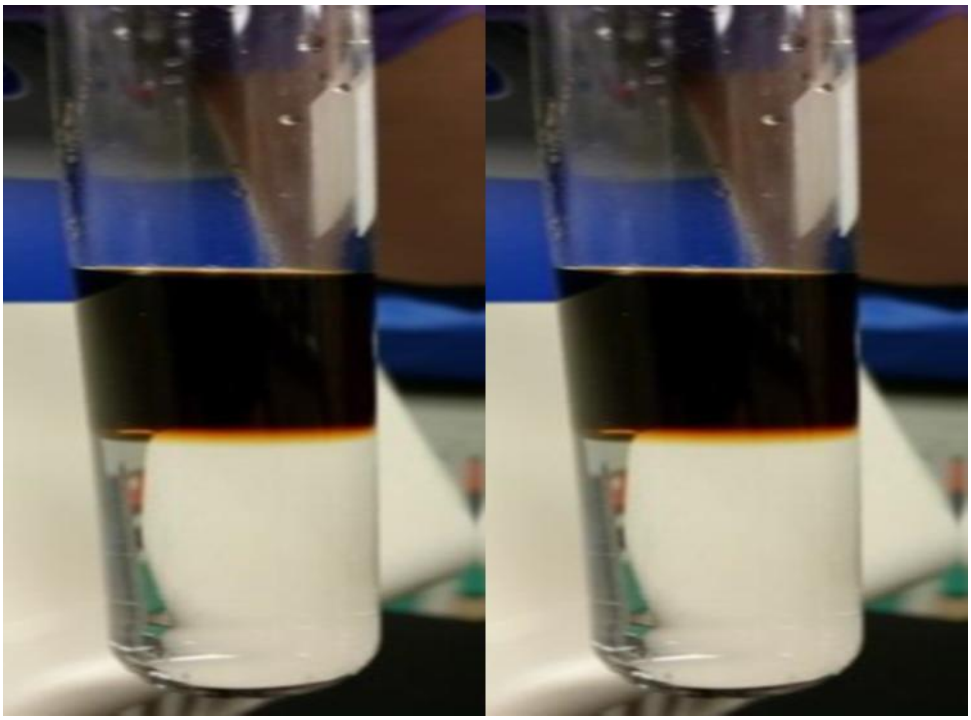

**Figure 4: MNPs Top Layer, PEG solution Bottom Layer**

### 3.6 Conjugation of Magnetic Nanoparticles (MNPs - EphA2)

The conjugation of MNPS to the EphA2 receptor was done based on the following procedures. A known weight of NHS and EDC were weighted in analytical balance separately followed by dissolving in distilled water in each test tube. EDC was pipetted and added to the PEG-coated sample solution. The solution was then allowed to react for 1 hour using a shaker.115 $\mu$L of NHS were pipetted into the above-reacted contents containing EDC and reacted for 15 minutes. A small volume EphA2 receptor was measured and added to 2mls of PBS. The solution was then allowed to react for four hours and characterized using UV-vis spectroscopy and FTIR spectroscopy.

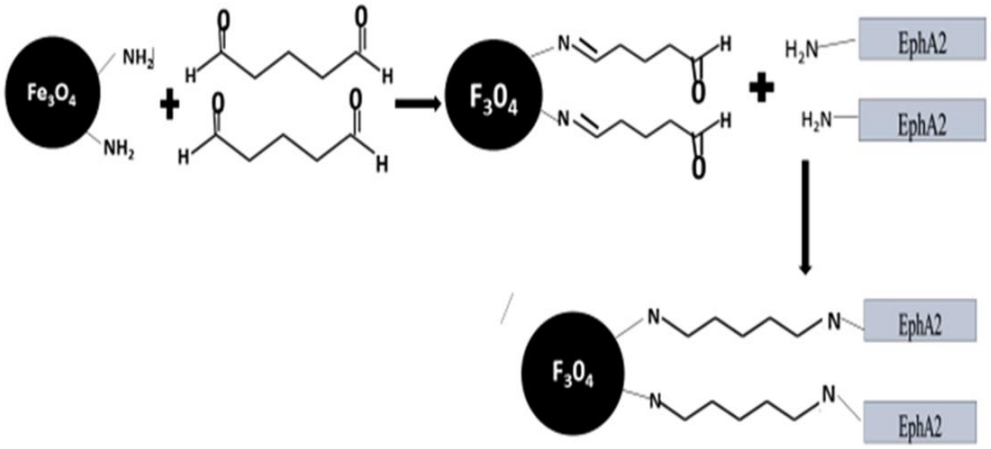


**Figure 5: Schematic pathway of EPHA2 conjugated to Nanoparticles**

### 3.7 Conjugation of LHRH-MNPS

1mg of LHRH was measured using a micropipette and dissolved in 1ml of PBS solvent. The measured solution was added to the PEGylated solution. The solution was allowed to react for 4 hours. The sample solution was characterized using FTIR and UV-vis techniques.

To make LHRH-MNPs, LHRH peptides were cross-linked to the surface of MNPs using glutaraldehyde cross-linking chemistry. The amine groups in LHRH peptides interacted with the remaining carbonyl groups in glutaraldehyde when they were incorporated into glutaraldehyde active MNPs. As a result, the carbonyl groups that were present in glutaraldehyde-activated MNPs vanished from the LHRH-MNPs' spectra, indicating that conjugation was efficient (Jingjie Hu et al., 2018).

As compared to their neutral or negatively charged counterparts, positively charged nanoparticles are usually taken up to a greater extent under higher cell phagocytosis rates.

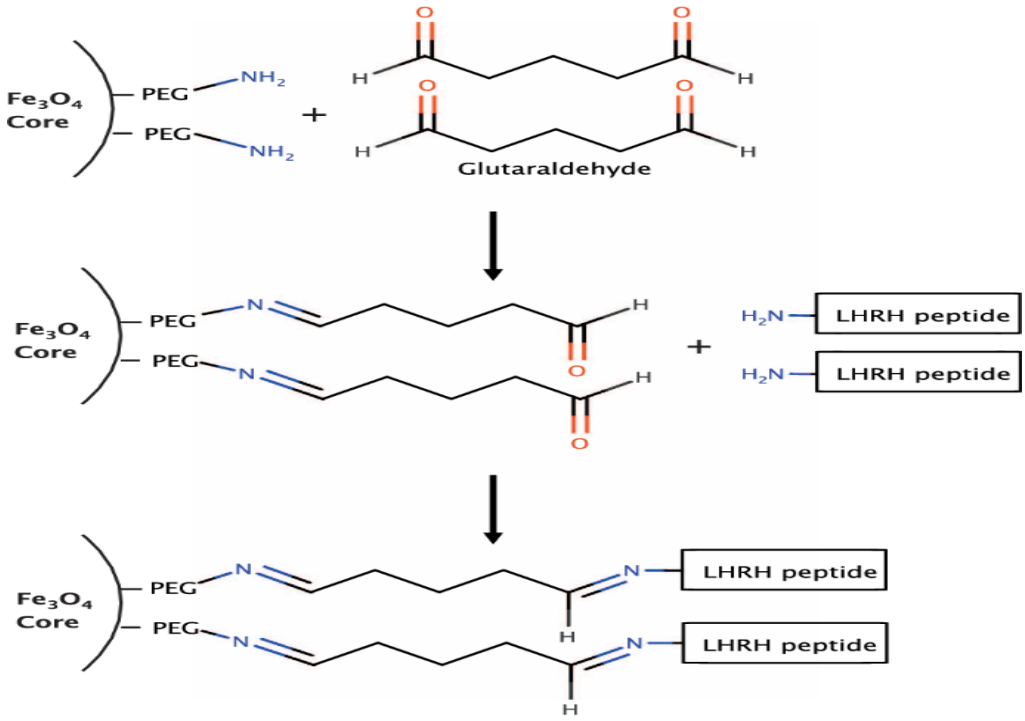


**Figure 6: Schematic of LHRH conjugated nanoparticles**

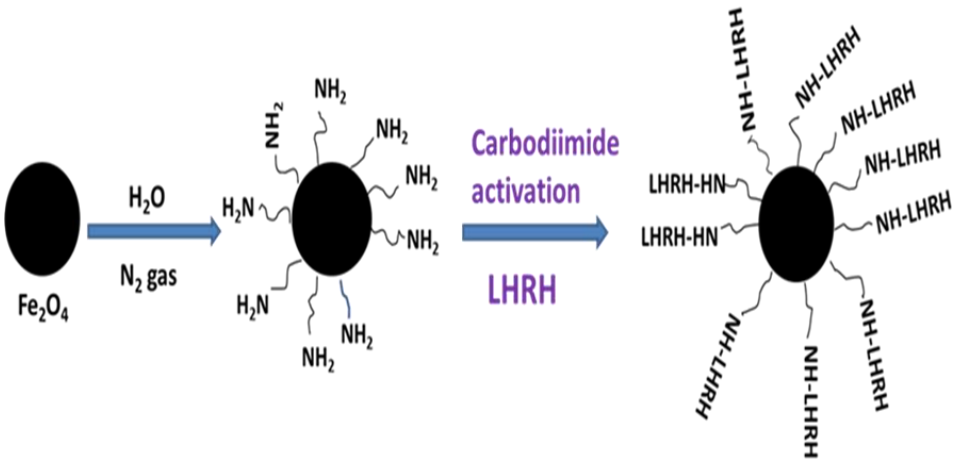


**Figure 7: Schematic of reaction pathway for the functionalization of MNPs with LHRH**

### 3.8 Characterization of Magnetite Nanoparticles (MNPs) and Conjugated Magnetite Nanoparticles

Pure MNPs, EphA2-MNPs, and LHRH-MNPs were characterized through several techniques, following established protocols.

Nanoparticle size and morphology were analyzed using Transmission Electron microscopy (TEM). The MNPs were analyzed using UV-vis spectroscopy (Specord 200 Plus, Germany) to determine the absorption peak and wavelength. The conjugated MNPS to LHRH and EphA2 were further analyzed using Fourier Transform Infrared Spectroscopy (FTIR) (Thermo Scientific Nicolet iS5, Germany) to determine the chemical composition of the nanoparticles before and after conjugation. A vibrating–sample magnetometer (VSM) was used to measure the magnetic properties of MNPs (Hu et al., 2020). The elemental composition of synthesized nanoparticles was determined using Energy Dispersive X-ray spectroscopy (EDS).

# CHAPTER FOUR

# RESULTS AND DISCUSSION

## 4.1 Introduction

This chapter presents results findings after characterization of nanoparticles on the structure of pure MNPs and EphA2 or LHRH conjugated to nanoparticles.

## 4.2 Nanoparticles Characterization

### 4.2.1 Nanoparticles analysis (synthesis and structure)

#### 4.2.1.1 Energy Dispersive X-ray spectroscopy (EDS)

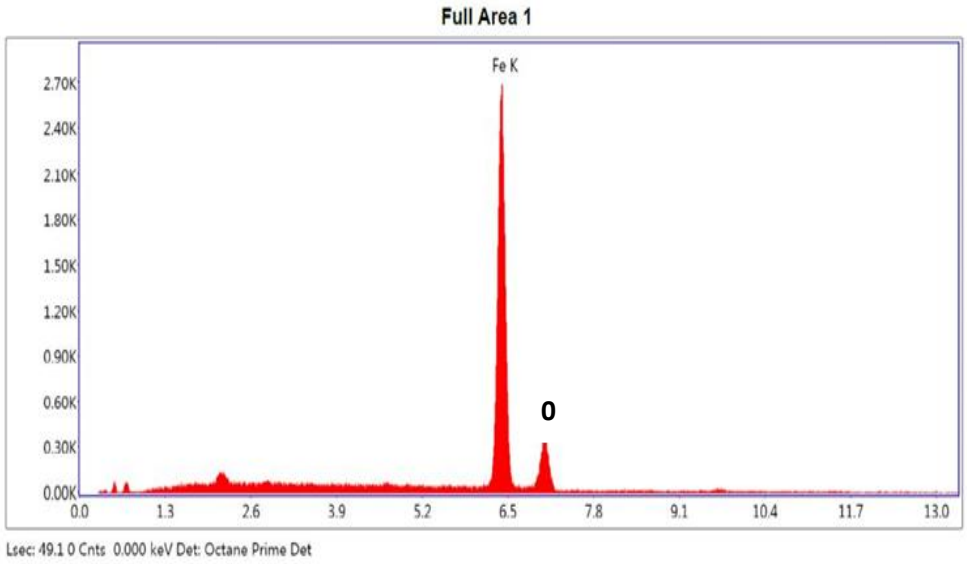


**Figure 8: EDS of synthesized magnetite nanoparticles**

EDS shows that synthesized nanoparticles rich in iron and oxygen elements observed in the dominant peak in Figure 8. Note that other minor elements shown by the short peaks are Carbon and Hydrogen due to coated oleic acid to the nanoparticles.

#### 4.2.1.2 Transmission Electron Microscopy (TEM)

TEM micrographs of the nanoparticles are presented in Figure 11. These show that the Magnetite nanoparticles are spherical and have core diameters ranging from 5 to 30nm range. This shows the synthesized magnetite nanoparticles size is within the range suitable for biomedical application. The histogram in Figure 10 shows core diameter distribution with a large number of nanoparticles size from 10nm to 35nm.

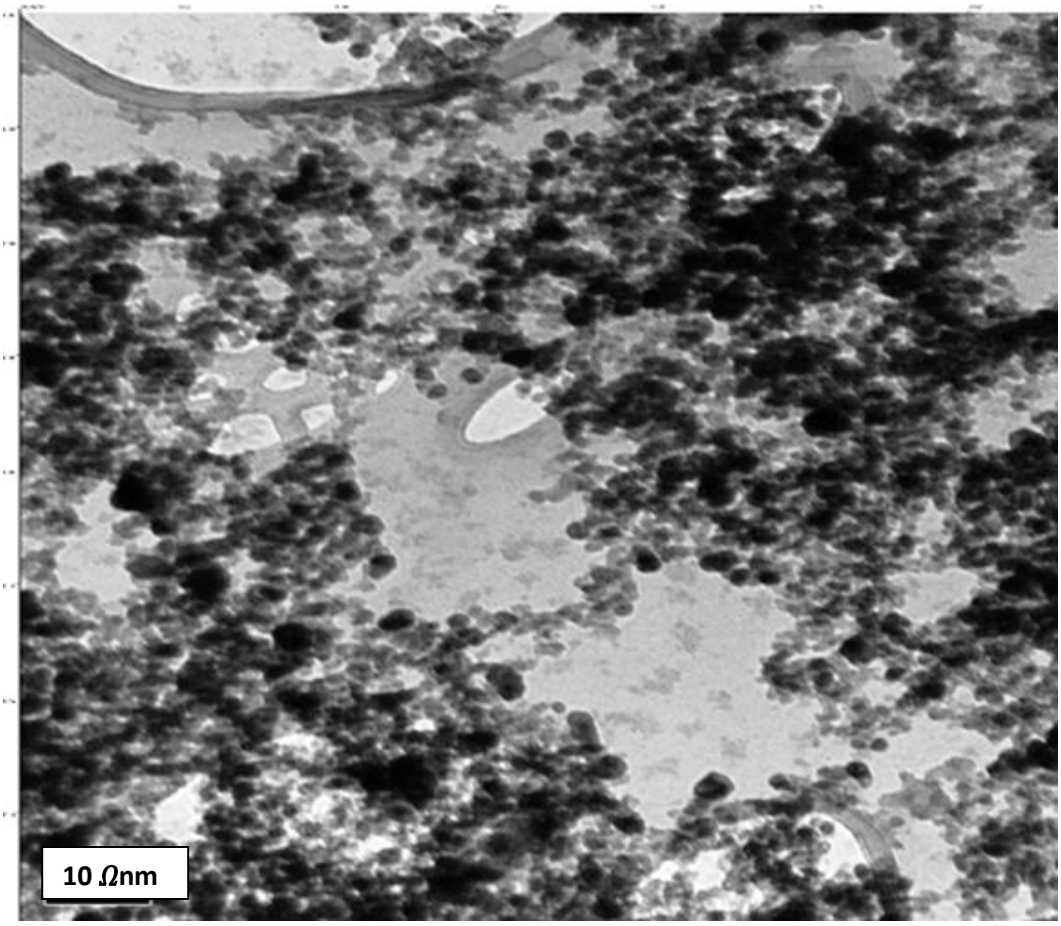


**Figure 9: TEM Micrograph of Synthesized Magnetite Nanoparticles**

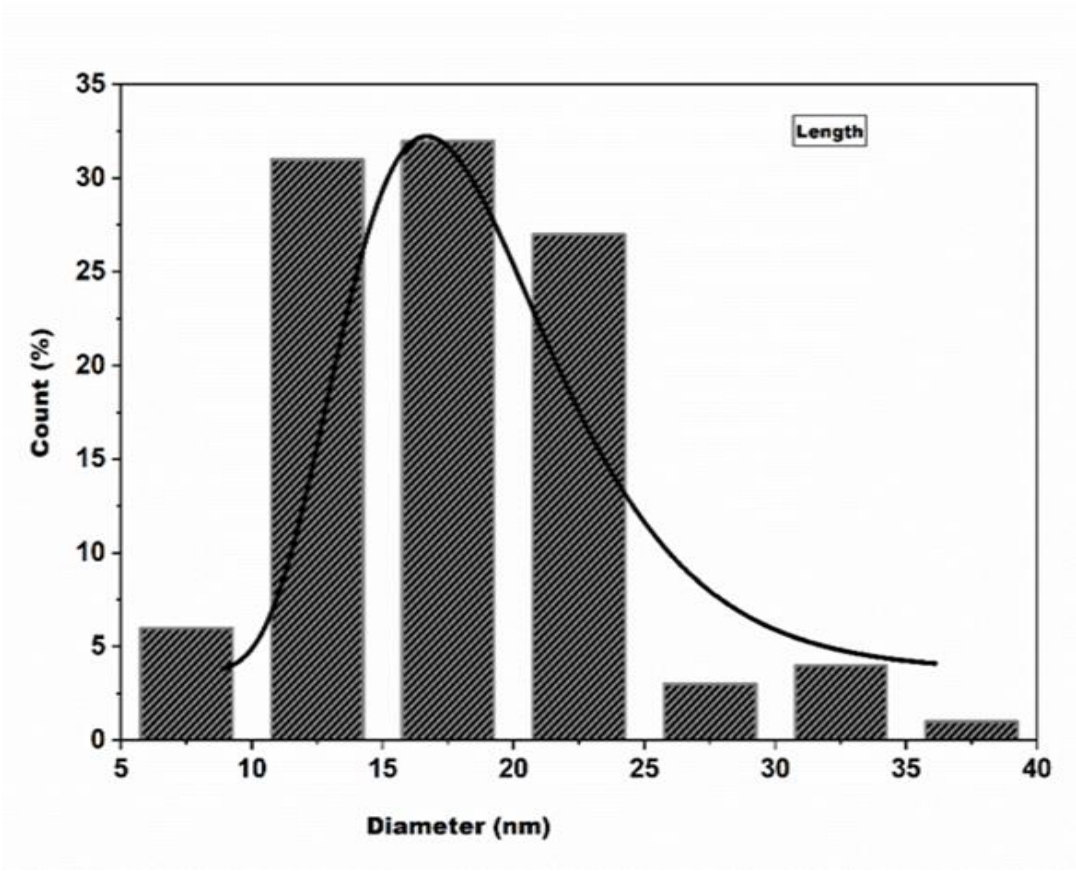


**Figure 10: Histogram core Diameter Distribution of Nanoparticles**

### 4.2.2 Magnetic Properties of MNPs

A vibrating sample magnetometer was used to investigate the magnetic properties of synthesized magnetite nanoparticles (VSM). Figure 11 shows typical moment versus magnetic field (M-H) plots for MNPs, displaying hysteresis loops estimated at 300 K in an applied magnetic field of up to 1000 kOe. MNPs have a saturation magnetization value of 2.67 emu/g.

Both values are very small when compared to the 92 emu/g stated for bulk $Fe_3O_4$. The decrease in saturation magnetization may be due to the small size of the nanoparticles, which lowers the relative mass ratio of the magnetic component (Jingjie Hu et al., 2020).

The magnetization curve in Figure 11 also shows that the nanoparticles are superparamagnetic, that is, on the application of an external magnetic field, they become magnetized up to their saturation magnetization, and on the removal of the magnetic field, they no longer exhibit any residual magnetic interaction. The particles are very small in size as the magnetic property depends on the sizes of the particles. Since these nanoparticles are so small, they don't have several domains like large magnets do; instead, they form a single magnetic domain and behave like a "single super spin" with a high magnetic susceptibility (Hoffmann et al., 2005).

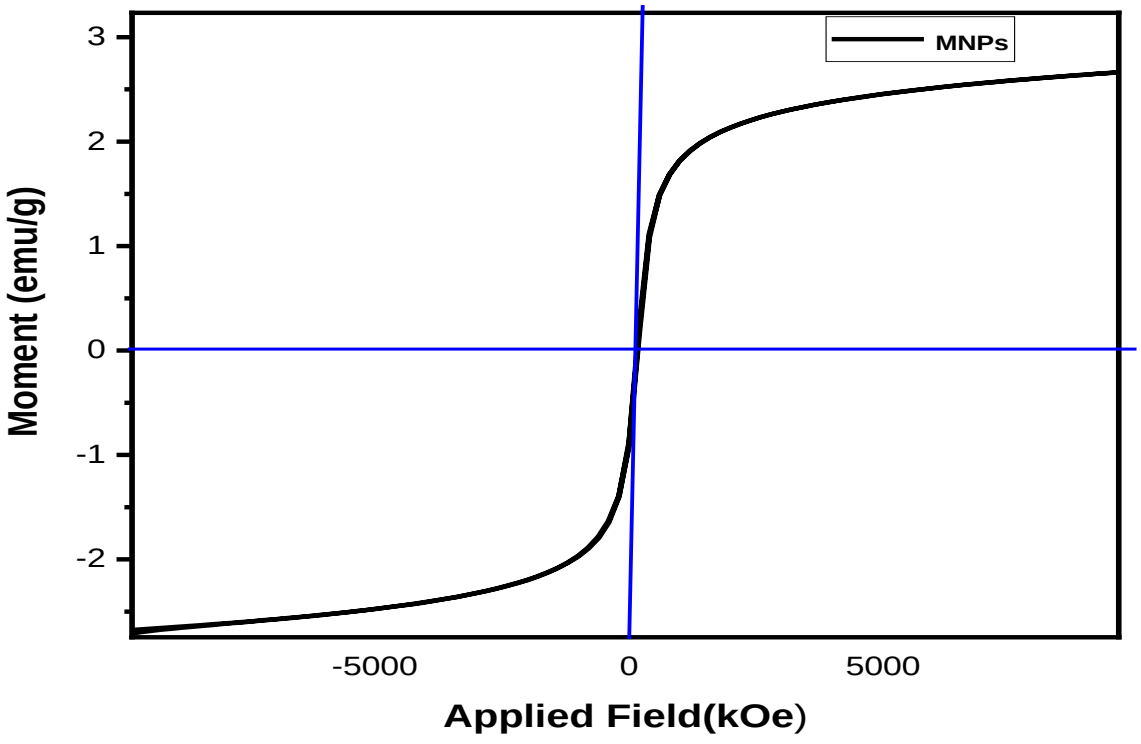


**Figure 11: Hysteresis loop for vibrating sample magnetometer (VSM) of MNPs with applied field ranging from -1000kOe to +1000kOe**

## 4.3 Characterization of Conjugated Nanoparticles

### 4.3.1 UV-vis spectroscopy

The UV-Vis spectra when Phosphate-Buffered Saline (PBS) solvent is used presented in Figures 12 – 15. These show high intensity absorbance bands for both PEGylated MNPs and pure MNPs, while the EphA2-conjugated MNPs spectra exhibit low absorbance bands. The synthesized magnetite nanoparticles absorb a UV-visible spectrum in the wavelength of 380nm, as shown in Figure 12. A narrow absorption band was observed at 978nm.

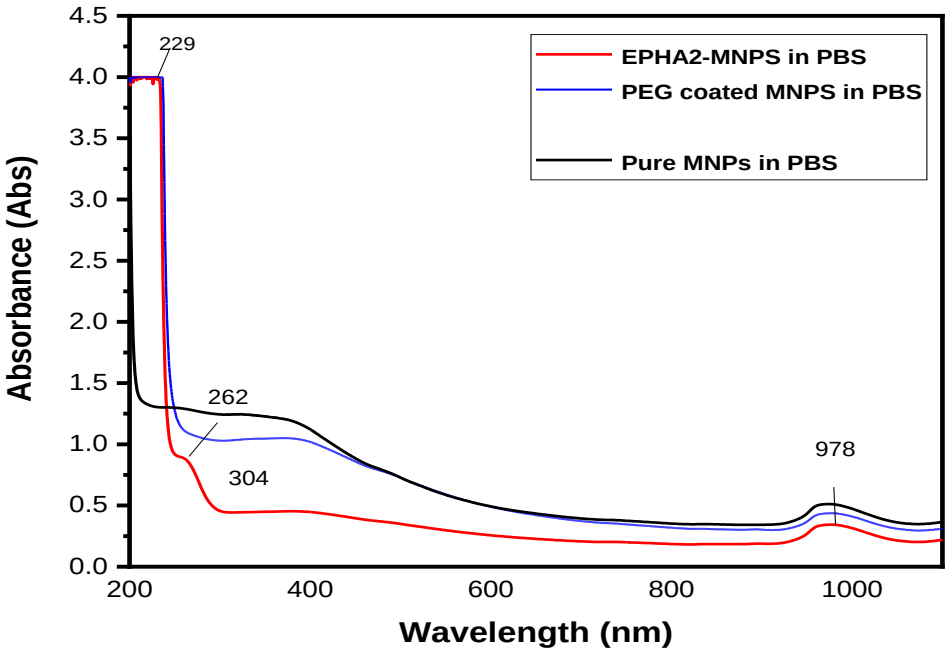


**Figure 12: UV-Vis spectroscopy of (a) EPHA2 conjugated nanoparticles (b) PEG-coated MNPs and (c) pure MNPs using phosphate Buffered Saline solvent**

When water is used as a solvent/ reference sample in Figures 13 and 14 EphA2 Conjugated magnetite nanoparticles (EphA2-MNPS) and LHRH-MNPs show low absorbance compared to PEGylated MNPs and pure MNPs. The broad absorption band is observed at wavelength 384nm for the PEG-coated MNPs spectrum.

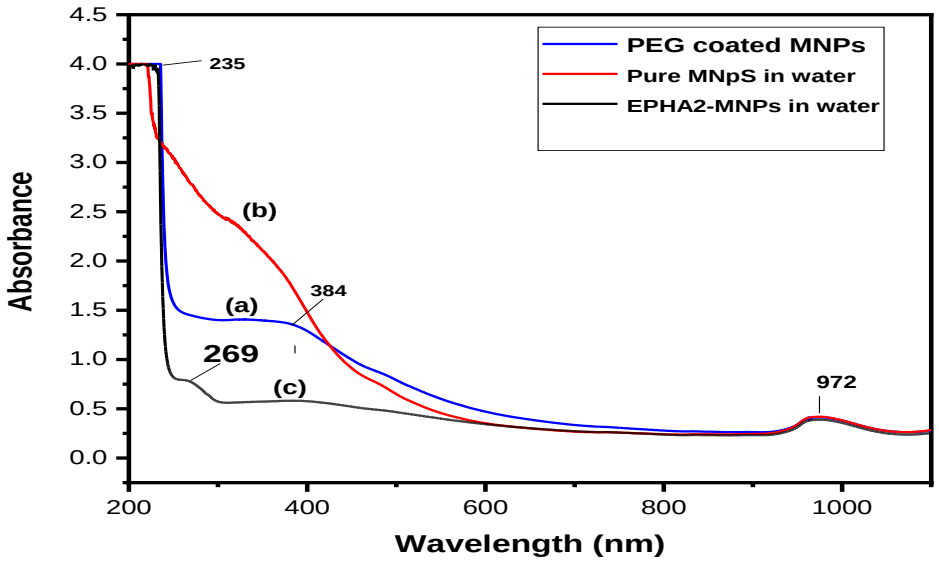


**Figure 13: UV-Vis spectroscope of (a) PEG-coated MNPs (b) pure magnetite nanoparticles and (c) EphA2 conjugated to MNPs using water solvent**

UV-Vis spectroscope analysis of PEG-coated nanoparticles reflects the broader peak at 384nm, the wavelength of light absorption for magnetite nanoparticles. Figure 13 reveals the minor absorption peak at 972 nm showing conjugation to nanoparticles. A similar characteristic pattern is observed from 500nm to 1100nm for EphA2-MNPs and LHRH-MNPs when water is used as a solvent.

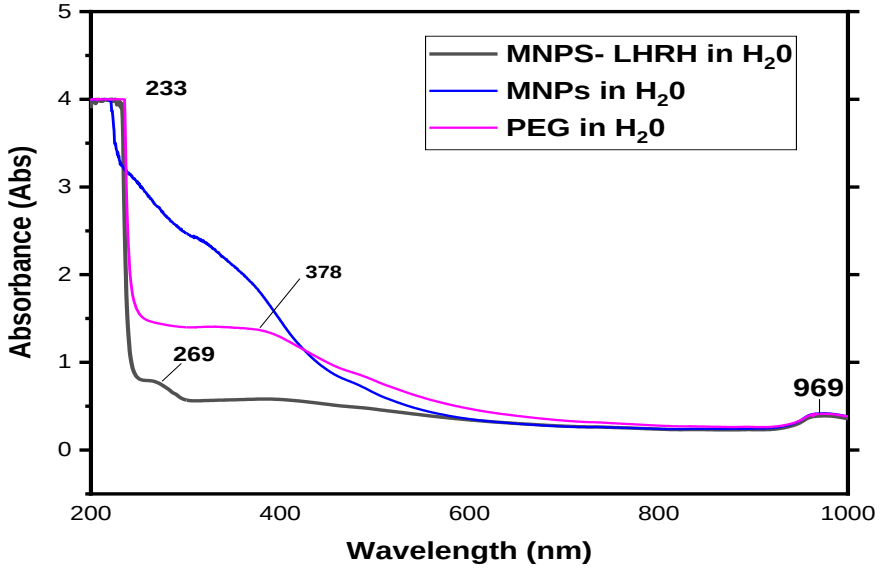


**Figure 14: UV-Vis of (a) LHRH conjugated nanoparticles, (b) pure magnetite, and(c) PEG-coated magnetite using water as a solvent**

In the case of the conjugation of nanoparticles using Phosphate-buffered saline (PBS) as a solvent, Figure 14 presents a low absorbance spectrum for Luteinizing Hormone Releasing-Hormone below that of pure MNPs and PEG-coated MNPs. Also, there is a similar characteristic pattern for the three spectra from 450 nm to 1100 nm. Furthermore, the conjugation of EphA2 and LHRH to magnetite nanoparticles using water (pH 5.8) gives higher absorbance compared to that of Phosphate Buffered Saline (pH 7.2). This suggests that, at high pH, there is lower absorbance than at lower pH

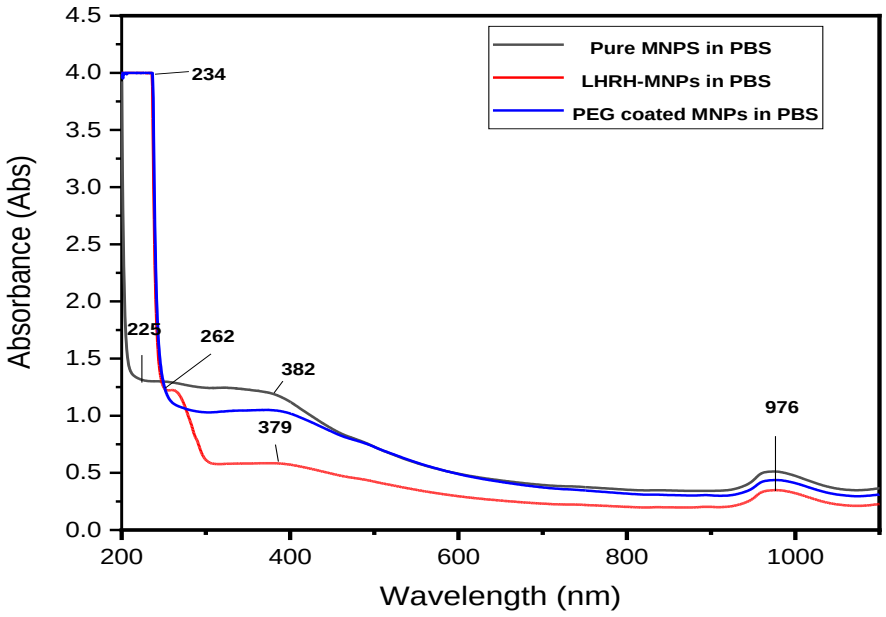


**Figure 15: UV-Vis of (a) pure MNPs (b) LHRH conjugated magnetite nanoparticles and (c) PEG-coated magnetite nanoparticles using Phosphate Buffered Saline solvent**

### 4.3.2 Fourier Transform Infrared (FT-IR) Spectroscopy

Fourier Transform Infrared (FTIR) spectroscopy was used to confirm the conjugation process. Figures 16, 17, and 18 present FTIR spectra for obtained for: (a) MNPs; (b) glutaraldehyde-activated MNPs; (c) LHRH-MNPs, and (d) EphA2-MNPs.

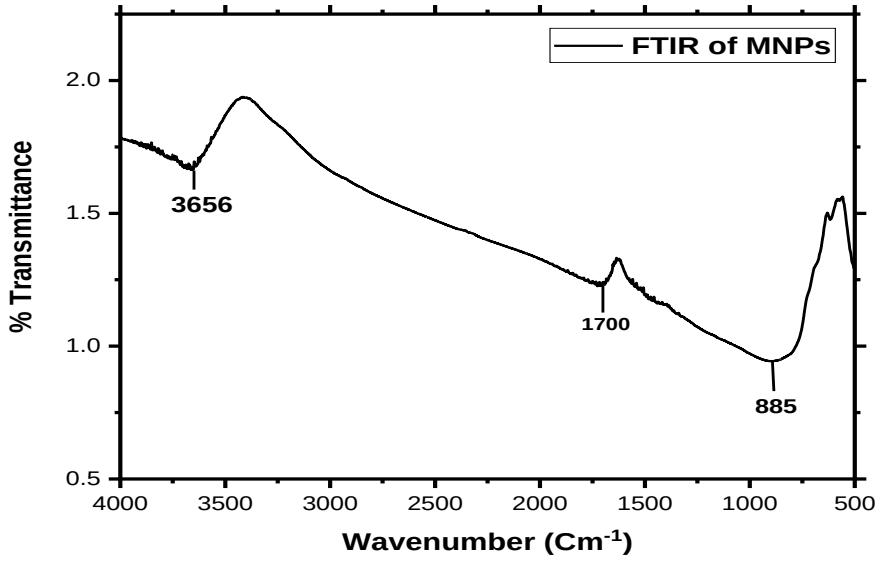


**Figure 16: FTIR spectra of pure magnetite**

FTIR spectra analysis of MNPs presented Peaks in Figure 16 were observed at 3656cm$^{-1}$, 1700cm$^{-1}$and 885cm,$^{-1}$ which corresponds at an–O-H stretch, -C=O stretch, This suggests that the broad and medium peak 3656cm$^{-1}$ is hydroxyl functional group found in magnetite nanoparticles coated with oleic acid.

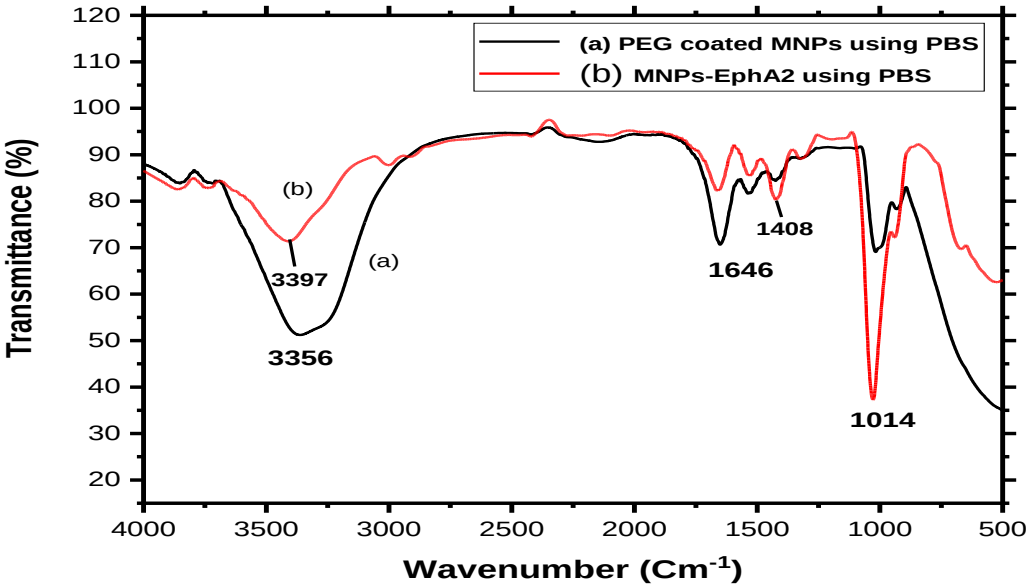


**Figure 17: FTIR spectra of (a) EphA2 conjugated to magnetite nanoparticles and (b) PEG-coated magnetite nanoparticles using PBS solvent**

From Figure 17 absorbance bands are observed at wavenumber 3356cm$^{-1}$, 1646cm$^{-1}$, 1408cm$^{-1}$ and 1014cm$^{-1}$. The medium and broad Peak 3356 cm$^{-1}$ is a characteristic peak of N-H stretch for the amine group. Absorbance bands 1646cm$^{-1}$, 1408, cm$^{-1}$ and 1014cm$^{-1}$ corresponds to C=0, and C-F. The N-H functional groups depict the EphA2 receptor structure made up of amino acids. The amide (-C=O) peak at 1646 cm$^{-1}$ shows that EphA2 was properly conjugated to MNPs.

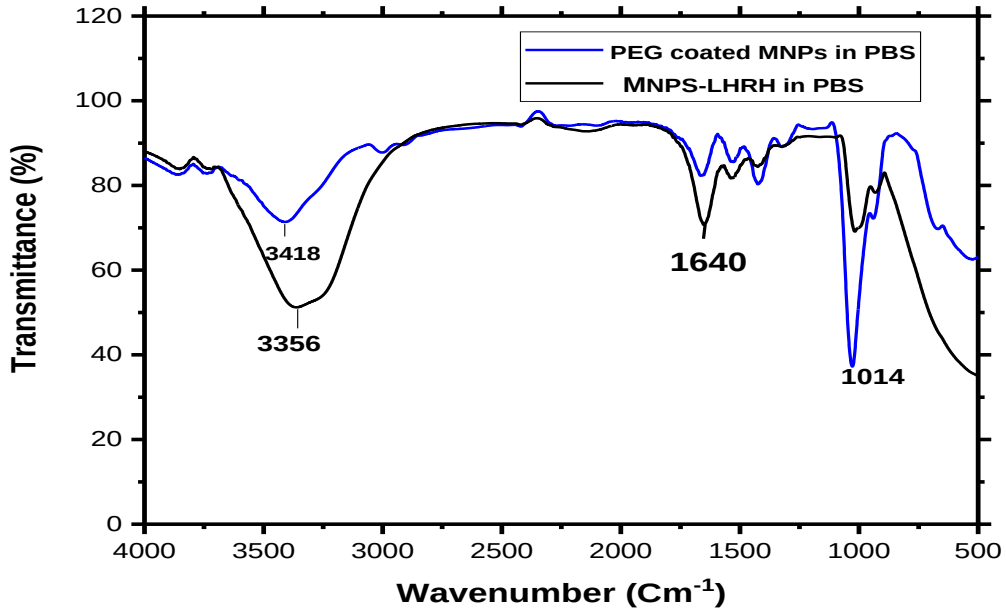


**Figure 18: FTIR spectra of (a) LHRH conjugated magnetite nanoparticles and (b) PEG-coated magnetite nanoparticles in PBS solvent**

FTIR spectra analysis of LHRH conjugated to MNPs in Figure 18 shows peak positions at 3356cm$^{-1}$, 1640cm$^{-1}$, 1014cm$^{-1}$, which corresponds at -N-H stretch, -C=0, and C-F stretch. The peak position at 3418 cm$^{-1}$ is a characteristic peak for -0-H stretch for oleic acid used during synthesis to stabilize the nanoparticles to prevent oxidation of nanoparticles to hematite.

This suggests that the broad peak 3356 $cm^{-1}$ is a characteristic absorption peak for the secondary amine (N-H) functional group that is found in the Luteinizing hormone Releasing hormone (LHRH). The 1640 nm is a characteristic peak of the amide group (-C=0) showing conjugation of magnetite to LHRH has taken place.

**4.4 Discussion**

All nanoparticles used for biomedical and bioengineering applications must have a scale smaller than 100 nm, with an average narrow particle size distribution/monodispersed, and superparamagnetic properties (Provenzano et al., 2009);(Shinkai et al., 1999);(Obayemi et al., 2015), according to The Royal Society and The Royal Academy of Engineering (2004). Figures 10 show the TEM findings for CMNPs synthesized at pH 7.0. The nanoparticles were mostly spherical, varying in diameter from 5 to 30 nm.

The Fourier Transform Infrared (FTIR) spectra of ligand conjugated biosynthesized iron oxide nanoparticles (BMNPs-LHRH) (in the transition mode) revealed a similar pattern with broad bands in the low-frequency field. The iron oxide skeleton is to blame for this (Zhou et al., 2006). The iron oxide spectra in other regions have weak bands. The spectra obtained between 4100 and 500 cm1 were found to be similar to magnetite ($Fe_3O_4$) (Gupta & Wells, 2004). FTIR spectral analysis of LHRH peptide bound magnetite nanoparticles also revealed the presence of characteristic bands of $–NH_2$ (3400 and 2850 cm−1) and the signatures of LHRH (Obayemi et al., 2015).

The saturation magnetization values of MNPs are 2.67 electromagnetic units per gram ($emu.g^{-1}$), according to hysteresis loops measured at 300 K in an applied magnetic field of up to 1000 kOe. This is a low value as compared to the 92 $emu.g^{-1}$ recorded for bulk iron

oxide $Fe_3O_4$. The decrease in saturation magnetization is likely due to the nanoparticles' small size, which lowers the magnetic component's relative mass ratio. This demonstrates that the synthesized MNPs have superparamagnetic properties, which are desirable for several biomedical applications.

Similar characteristics were observed in the magnetization curves that were obtained from the biologically synthesized magnetite nanoparticles with saturation magnetization of 2.5 emu/g Fe compared to the bulk 90 emu/g (Obayemi et al., 2015). However, the saturation magnetization levels of the chemically synthesized magnetite were much greater than those of the biosynthesized magnetite. Furthermore, when the applied magnetic fields were withdrawn, both chemically synthesized and biosynthesized magnetite nanoparticles showed negligible hysteresis in their magnetization curves, which decreased from saturation values to almost zero (negligible residual magnetization) (Obayemi et al., 2015).

The UV-Vis results presented in Figures 12 -15 show that a broader absorption band was observed for wavelengths in the range between 250 nm and 440 nm. Lower absorbance bands were observed in both EphA2-conjugated to MNPs and LHRH-conjugated MNPs. Unlike the biosynthesis of nanoparticles, the chemical synthesis method results in a high production yield of nanoparticles. Also, the conditions for synthesis are simple and easy to scale-up. Such ease of scale up has facilitated the approval by the U.S. Food and Drug Administration (FDA) of this process as method for producing MRI contrast agents (Hernández-Hernández et al., 2020).

# CHAPTER FIVE

# SUMMARY AND CONCLUSION

## 5.1 Introduction

This chapter provides a summary of the major findings obtained from this study. Recommendations for future work are also presented.

## 5.2 Summary

Iron Chloride was used for the chemical synthesis of magnetite nanoparticles with sizes between 5nm and 30nm. The reaction between ferric chloride and ferrous chloride was precipitated by the addition of Sodium Hydroxide (NaOH). The formation of magnetite nanoparticles was confirmed via EDS and VSM technique showing elemental composition and magnetic property, respectively. Two broad and sharp peaks were observed in EDS analysis composed of iron and oxygen, elements found in MNPs.

UV–Visible spectroscopy was used to identify magnetite at a wavelength of ~384 nm. FTIR was also used to show that magnetite nanoparticles were successfully conjugated to LHRH and EpHA2. Subsequent TEM studies of the magnetite nanoparticles revealed that the particles were spherical shape, with sizes between 5 and 30 nm that are needed for applications in MRI contrast agents and nanoparticles for hyperthermic cancer treatment.

VSM was used to study the magnetic properties of the MNPs. There was no diamagnetic contribution to the superparamagnetic behavior of the particles. They are particularly interesting because they lose their magnetism when a magnetic field is removed. They can also enable enhanced MRI imaging and potential applications in localized hyperthermia.

The FTIR results presented also confirm that the LHRH and EphA2 ligands are chemically bound to the magnetite nanoparticles through amines. The LHRH-conjugated magnetite nanoparticles may be suitable for potential applications in the detection and targeted treatment of breast cancer.

### 5.3 Conclusions

In this study, we synthesized spherical MNPs with sizes ranging between 5nm to 30nm through the co-precipitation method to improve cell biocompatibility. The PEG molecules were successfully coated on the surface of MNPs, as revealed by FTIR and UV-vis spectroscopy to prevent nanoparticle agglomeration. From the subsequent data acquired from TEM, VSM, UV-VIS Spectroscopy the MNPs were confirmed to be monodisperse and superparamagnetic. Taken together, we have synthesized and characterized MNPs and LHRH/EphA2 conjugated MNPs as a novel, superparamagnetic and biocompatible material that has a potential application as magnetic carriers for breast cancer detection or treatment.

### 5.4 Recommendations for Future Work

This study explores the synthesis and characterization of functionalized magnetite nanoparticles for targeting breast cancer cells. Experiments on functionalized magnetite nanoparticles to target breast cancer cells were not carried out because of time constraints, limited project funds, and the COVID-19 pandemic, which resulted in difficulties in accessing laboratory facilities. There are recommended for future work.

The zeta potential technique should also be used to determine surface charges of nanoparticles, and hence determine the dispersion stability. In-vivo studies are needed to

study the effects of chemically synthesized nanoparticles with those of biosynthesized MNPs on MRI contrast and potential hyperthermic effects that can be induced by laser interactions or the controlled application of magnetic fields.

There is a need to study the effects of magnetite nanoparticles with rod-shaped and non-spherical morphologies. Such shapes can change the MRI contrast, as well as the potential hyperthermic heating that can be achieved by the application of magnetic fields, as well as interactions with laser beams.

There is the potential to find out how the size of MNPs and electrostatic potential depends on pH and ionic strength of the precipitating solution. Further research is also needed to develop a basic understanding of how nucleation and growth processes (in biochemical environments) affect MNPs shape and size. Finally, there is a need for further research to study the potential toxicity effects associated with the nanoparticles that were presented in this study.

## REFERENCES

*Advanced breast cancer : diagnosis and treatment*. (2020). *February 2009*.

Aldhaeebi, M. A., Alzoubi, K., Almoneef, T. S., Bamatra, S. M., Attia, H., & Ramahi, O. M. (2020). Review of microwaves techniques for breast cancer detection. *Sensors (Switzerland)*, *20*(8), 1–38. https://doi.org/10.3390/s20082390

Anders, C. K., & Carey, L. A. (2009). Biology, metastatic patterns, and treatment of patients with triple-negative breast cancer. *Clinical Breast Cancer*, *9*(SUPPL.2). https://doi.org/10.3816/CBC.2009.s.008

Andersson, M., Lidbrink, E., Bjerre, K., Wist, E., Enevoldsen, K., Jensen, A. B., Karlsson, P., Tange, U. B., Sørensen, P. G., Møller, S., Bergh, J., & Langkjer, S. T. (2011). Phase III randomized study comparing docetaxel plus trastuzumab with vinorelbine plus trastuzumab as first-line therapy of metastatic or locally advanced human epidermal growth factor receptor 2-positive breast cancer: The HERNATA study. *Journal of Clinical Oncology*, *29*(3). https://doi.org/10.1200/JCO.2010.30.8213

Anuku, N., Obayemi, J. D., Odusanya, O. S., Malatesta, K. A., & Soboyejo, W. (2020). *Bioinspired Design of Nanostructures Inspiration from Viruses for Disease Detection and Treatment*. 212–232.

Bao, Y., Sherwood, J. A., & Sun, Z. (2018). Magnetic iron oxide nanoparticles as: T 1 contrast agents for magnetic resonance imaging. In *Journal of Materials Chemistry C* (Vol. 6, Issue 6). https://doi.org/10.1039/c7tc05854c

Collignon, J., Lousberg, L., Schroeder, H., & Jerusalem, G. (2016). Triple-negative breast cancer: Treatment challenges and solutions. *Breast Cancer: Targets and Therapy*, *8*, 93–107. https://doi.org/10.2147/BCTT.S69488

Ganapathe, L. S., Mohamed, M. A., Yunus, R. M., & Berhanuddin, D. D. (2020). Magnetite (Fe3O4) nanoparticles in biomedical application: From synthesis to surface functionalisation. In *Magnetochemistry* (Vol. 6, Issue 4). https://doi.org/10.3390/magnetochemistry6040068

Gegechkori, N., Haines, L., & Lin, J. J. (2017). Long-Term and Latent Side Effects of Specific Cancer Types. In *Medical Clinics of North America* (Vol. 101, Issue 6). https://doi.org/10.1016/j.mcna.2017.06.003

Gelmon, K. A., Boyle, F. M., Kaufman, B., Huntsman, D. G., Manikhas, A., Di Leo, A., Martin, M., Schwartzberg, L. S., Lemieux, J., Aparicio, S., Shepherd, L. E., Dent, S., Ellard, S. L., Tonkin, K., Pritchard, K. I., Whelan, T. J., Nomikos, D., Nusch, A., Coleman, R. E., … Parulekar, W. R. (2015). Lapatinib or trastuzumab plus taxane therapy for human epidermal growth factor receptor 2-positive advanced breast cancer: Final results of NCIC CTG MA.31. *Journal of Clinical Oncology*, *33*(14). https://doi.org/10.1200/JCO.2014.56.9590

Gupta, A. K., & Wells, S. (2004). Surface-Modified Superparamagnetic Nanoparticles for Drug Delivery: Preparation, Characterization, and Cytotoxicity Studies. *IEEE Transactions on Nanobioscience*, *3*(1). https://doi.org/10.1109/TNB.2003.820277

Hampp, E., Botah, R., Odusanya, O. S., Anuku, N., Malatesta, K. A., & Soboyejo, W. O. (2012). Biosynthesis and adhesion of gold nanoparticles for breast cancer detection and treatment. *Journal of Materials Research*, *27*(22). https://doi.org/10.1557/jmr.2012.317

Helms, C. R. (1983). Materials Characterization. *NATO ASI Series, Series E: Applied Sciences*, *62*, 210–225. https://doi.org/10.1007/978-94-009-6842-4_6

Hernández-Hernández, A. A., Aguirre-Álvarez, G., Cariño-Cortés, R., Mendoza-Huizar, L. H., & Jiménez-Alvarado, R. (2020). Iron oxide nanoparticles: synthesis, functionalization, and applications in diagnosis and treatment of cancer. *Chemical Papers*, *74*(11), 3809–3824. https://doi.org/10.1007/s11696-020-01229-8

Hoffmann, H., Petri-Fink, A., Steitz, B., Von Rechenberg, B., Hofmann, M., & Juillerat, J. (2005). Superparamagnetic iron oxide nanoparticles for multiple biomedical applications. *2005 NSTI Nanotechnology Conference and Trade Show - NSTI Nanotech 2005 Technical Proceedings*.

Hu, J, Obayemi, J. D., Malatesta, K., Ko, A., & Soboyejo, W. O. (2018). *Materials Science & Engineering C Enhanced cellular uptake of LHRH-conjugated PEG-coated magnetite nanoparticles for speci fi c targeting of triple negative breast cancer cells*. *88*(July 2017), 32–45. https://doi.org/10.1016/j.msec.2018.02.017

Hu, Jingjie, Obayemi, J., Malatesta, K., Yurkow, E., Adler, D., & Soboyejo, W. (2020). Luteinizing hormone-releasing hormone (LHRH) conjugated magnetite nanoparticles as MRI contrast agents for breast cancer imaging. *Applied Sciences (Switzerland)*, *10*(15), 1–18. https://doi.org/10.3390/app10155175

Hu, Jingjie, Youssefian, S., Obayemi, J., Malatesta, K., Rahbar, N., & Soboyejo, W. (2018). Investigation of Adhesive Interactions in the Specific Targeting of Triptorelin-conjugated PEG-coated Magnetite Nanoparticles to Breast Cancer Cells. *Acta Biomaterialia*. https://doi.org/10.1016/j.actbio.2018.02.011

Ismail-khan, R., & Bui, M. M. (2014). *A Review of Triple-Negative Breast Cancer A Review of Triple-Negative Breast Cancer*. *May*. https://doi.org/10.1177/107327481001700305

Medina, M. A., Oza, G., Sharma, A., Arriaga, L. G., Hern, M., Rotello, V. M., & Ramirez, J. T. (2020). *Triple-Negative Breast Cancer : A Review of Conventional and Advanced Therapeutic Strategies*. 1–32.

Meng, J., Fan, J., Galiana, G., Branca, R. T., Clasen, P. L., Ma, S., Zhou, J., Leuschner, C., Kumar, C. S. S. R., Hormes, J., Otiti, T., Beye, A. C., Harmer, M. P., Kiely, C. J., Warren, W., Haataja, M. P., & Soboyejo, W. O. (2009). LHRH-functionalized superparamagnetic iron oxide nanoparticles for breast cancer targeting and contrast enhancement in MRI. *Materials Science and Engineering C*, *29*(4). https://doi.org/10.1016/j.msec.2008.09.039

Nazário, A. C. P., Facina, G., & Filassi, J. R. (2015). Breast cancer: News in diagnosis and treatment. In *Revista da Associacao Medica Brasileira* (Vol. 61, Issue 6). https://doi.org/10.1590/1806-9282.61.06.543

Obayemi, J D, Dozie-nwachukwu, S., Danyuo, Y., Odusanya, O. S., & Anuku, N. (2015). Biosynthesis and the conjugation of magnetite nanoparticles with luteinizing hormone releasing hormone ( LHRH ). *Materials Science & Engineering C*, *46*, 482–496. https://doi.org/10.1016/j.msec.2014.10.081

Obayemi, John D., Hu, J., Uzonwanne, V. O., Odusanya, O. S., Malatesta, K., Anuku, N., & Soboyejo, W. O. (2017). Adhesion of ligand-conjugated biosynthesized magnetite nanoparticles to triple negative breast cancer cells. *Journal of the Mechanical Behavior of Biomedical Materials*, *68*, 276–286. https://doi.org/10.1016/j.jmbbm.2017.02.004

Press, D. (2012). *Superparamagnetic iron oxide nanoparticles : magnetic nanoplatforms as drug carriers*. 3445–3471.

Provenzano, R., Schiller, B., Rao, M., Coyne, D., Brenner, L., & Pereira, B. J. G. (2009). Ferumoxytol as an intravenous iron replacement therapy in hemodialysis patients. *Clinical Journal of the American Society of Nephrology*, *4*(2). https://doi.org/10.2215/CJN.02840608

Revia, R. A., & Zhang, M. (2016). Magnetite nanoparticles for cancer diagnosis, treatment, and treatment monitoring: Recent advances. In *Materials Today* (Vol. 19, Issue 3). https://doi.org/10.1016/j.mattod.2015.08.022

Section, S., & Epidemic, T. O. (2018). *Estimated number of new cancer cases, all EU countries, 2018*. https://doi.org/10.1787/health_glance_eur-2018-graph47-en

Sharma, K. S., Ningthoujam, R. S., Dubey, A. K., Chattopadhyay, A., & Phapale, S. (2018). Synthesis and characterization of monodispersed water dispersible Fe 3 O 4 nanoparticles and in vitro studies on human breast carcinoma cell line under hyperthermia condition. *Scientific Reports, January 2016*, 1–11. https://doi.org/10.1038/s41598-018-32934-w

Shekar, N., Mallya, P., Gowda, D. V., & Jain, V. (2020). Triple-negative breast cancer: Challenges and treatment options. *International Journal of Research in Pharmaceutical Sciences*, *11*(2). https://doi.org/10.26452/ijrps.v11i2.2127

Shinkai, M., Yanase, M., Suzuki, M., Hiroyuki Honda, Wakabayashi, T., Yoshida, J., & Kobayashi, T. (1999). Intracellular hyperthermia for cancer using magnetite cationic liposomes. *Journal of Magnetism and Magnetic Materials*, *194*(1). https://doi.org/10.1016/S0304-8853(98)00586-1

Slamon, D. J., Leyland-Jones, B., Shak, S., Fuchs, H., Paton, V., Bajamonde, A., Fleming, T., Eiermann, W., Wolter, J., Pegram, M., Baselga, J., & Norton, L. (2001). Use of Chemotherapy plus a Monoclonal Antibody against HER2 for Metastatic Breast Cancer That Overexpresses HER2. *New England Journal of Medicine*, *344*(11). https://doi.org/10.1056/nejm200103153441101

Stephen, Z. R., Kievit, F. M., & Zhang, M. (2011). Magnetite nanoparticles for medical MR imaging. *Materials Today*, *14*(7–8). https://doi.org/10.1016/S1369-7021(11)70163-8

Wahajuddin, & Arora, S. (2012). Superparamagnetic iron oxide nanoparticles: Magnetic nanoplatforms as drug carriers. In *International Journal of Nanomedicine* (Vol. 7). https://doi.org/10.2147/IJN.S30320

Zhang, Y., Kohler, N., & Zhang, M. (2002). Surface modification of superparamagnetic magnetite nanoparticles and their intracellular uptake. *Biomaterials*, *23*(7). https://doi.org/10.1016/S0142-9612(01)00267-8

Zhang, Y., Sun, C., Kohler, N., & Zhang, M. (2004). Self-assembled coatings on individual monodisperse magnetite nanoparticles for efficient intracellular uptake. *Biomedical Microdevices*, *6*(1). https://doi.org/10.1023/B:BMMD.0000013363.77466.63

Zhang, Y., & Zhang, J. (2005). Surface modification of monodisperse magnetite nanoparticles for improved intracellular uptake to breast cancer cells. *Journal of Colloid and Interface Science*, *283*(2). https://doi.org/10.1016/j.jcis.2004.09.042

Zhou, J., Leuschner, C., Kumar, C., Hormes, J., & Soboyejo, W. O. (2006). *A TEM study of functionalized magnetic nanoparticles targeting breast cancer cells*. *26*, 1451–1455. https://doi.org/10.1016/j.msec.2005.08.027